Potential Functions and Static and Dynamic Properties of Mg^{m+}Ar$_n$ ($m = 1, 2$; $n = 1-18$) Clusters

G. S. Fanourgakis and S. C. Farantos*

Institute of Electronic Structure and Laser, Foundation for Research and Technology−Hellas, and Department of Chemistry, University of Crete, Iraklion, Crete 711 10, Greece

Analytical potential functions have been constructed for Mg^{m+}Ar$_n$, m=1, 2, clusters by combining ab initio calculations with the electrostatic model of ion−induced dipole and induced dipole−induced dipole interactions. The most stable structures and dynamic properties are investigated by molecular dynamics techniques. For Mg$^+$Ar$_{12}$ an icosahedral geometry is predicted. For Mg$^+$Ar$_n$ clusters with $n = 7-12$ two series of minima with small differences in energy were found; in one the magnesium ion stays inside the cluster (solvated) and in the other on the surface of the system. For $n > 9$, clusters with Mg on the surface are slightly more stable and have a distinguishable high vibrational frequency relative to those with the magnesium ion inside. We find no such trends for Mg^{2+}Ar$_n$ clusters, in which the Mg cation is always solvated. The absolute minimum of Mg^{2+}Ar$_4$ is a regular tetrahedron, and that of Mg^{2+}Ar$_6$, a regular octahedron. The stability of all these clusters is investigated by studying caloric curves, root mean square bond length fluctuations, radial distributions, and power spectra.

1. Introduction

The interest in investigating the structures and dynamical properties of small finite systems such as atomic and molecular clusters[1] has led theoretical work to the study of several kinds of forces exerted among the atoms: van der Waals,[2] hydrogen bonding,[3−6] metallic,[7] ionic,[8,9] and covalently bonding[10−12] clusters have been explored.

Ionic clusters are particularly favored in experimental studies, since they are directly detected by a mass spectrometer. Thus, metal ions interacting with inert gases serve as proper models for studying solvation effects and, generally, the dependence of the properties of the clusters on their sizes.[1]

The work presented in this article has been motivated by the recent experimental investigation of Mg$^+$Ar$_n$ and Mg^{2+}Ar$_n$ clusters by Velegrakis and Lüder.[13] These researchers used the laser ablation technique to form metal cations which were ejected into a supersonic jet of argon. It is believed that the clusters are formed at the early stage of the adiabatic expansion by addition of Ar atoms to the smaller size clusters. The highly energized species were cooled by collisions, and the final products were detected by a time of flight apparatus.

From the analysis of the mass spectra some particularly stable structures (known as magic numbers) were detected for both types of clusters. Mg$^+$Ar$_n$ yielded higher intensity peaks relative to the neighboring ones for $n = 12$, 18, 22, 25, 28, 31, 45, and 54, whereas Mg^{2+}Ar$_n$ gave markedly different behavior, showing only one sharp peak at $n = 6$ and a broad peak at $n = 14$.[13]

The magic numbers of the monopositive clusters coincide with those of pure argon clusters.[14] This led to the speculation that the structures of Mg$^+$Ar$_n$ are the same as those of Ar$_{n+1}$ clusters. The structure of Ar$_{13}$ is that of a regular icosahedron which has an argon atom in the center, and larger magic number aggregates are formed with the construction of additional regular pentagons. For the double-charged magnesium−argon complexes an octahedral and a fcc type geometry were conjectured for $n = 6$ and 14, respectively.

The ionic character of magnesium and the number of electrons in this species allow for detailed experiments and accurate

theoretical calculations of the small aggregates of the magnesium cation with inert gases. Indeed, Pilgrim et al.[15] have recently studied the photodissociation spectroscopy of species Mg$^+$M (M = Ar, Kr, Xe). Vibrational frequencies, dissociation energies, and spin−orbit splittings were measured. Their results have been reanalyzed by Le Roy[16] using near dissociation theories in order to obtain improved estimates of the dissociation energies.

Bauschlicher and co-workers[17−19] have carried out high-level ab initio calculations for Mg$^+$Ar and Mg$^+$Ar$_2$ complexes. They concluded that the nature of the interaction is mainly electrostatic. The calculated dissociation energy of Mg$^+$Ar (3.25 kcal/mol) is in good agreement with the spectroscopically estimated one (3.66 kcal/mol). In a recent article Bauschlicher and Partridge[20] calculated the ground and the electronically excited states of Mg$^+$Ar and Mg$^+$Kr and made a direct comparison with the experimental results of Pilgrim et al.[15] Good agreement between computed and experimental results was found.

Density functional theory has been applied by Eriksson[21] to compute equilibrium geometries, energetics, and hyperfine coupling constants for a number of charged magnesium clusters and magnesium−rare gas complexes in matrices.

Patil[22] analyzed the interactions of inert gases with closed shell alkali and alkaline earth ions using a perturbative approach. He predicted a binding energy for Mg^{2+}Ar of 45 kcal/mol and a bond length of 3.78 a_0.

The recent production of larger mono- and double-charged magnesium−argon clusters[13] calls for further theoretical work on these systems. It is interesting to find the minimum energy geometries and compare their dynamical properties in parallel for the mono- and double-charged metal ion. In this article we undertake such a study.

To investigate large clusters, we construct analytical potential functions based on the electrostatic asymptotic expansion model[8] and utilize the ab initio results for the small clusters. For the monocation we use Partridge et al.'s[19] calculations, but for Mg^{2+} we perform self-consistent-field (SCF) computations in association with Møller Plesset[23] second order perturbation (MP2) calculations. We indeed confirm the icosahedral geom-

Potential Functions of $Mg^{m+}Ar_n$ ($m = 1, 2$; $n = 1-18$) Clusters

J. Phys. Chem., Vol. 100, No. 10, 1996 **3901**

etry of Mg^+Ar_{12} and the extra stability of this cluster implied from the mass spectrum. However, the interesting finding of the present study is the prediction that the Mg ion may sit either in the interior of the cluster or on the surface. For $Mg^{2+}Ar_6$ a regular octahedron of O_h symmetry is predicted.

The article is organized as follows: In section 2 we describe the potential energy surfaces (pes), in section 3 we describe the minimum energy geometries for different size Ar clusters, in section 4 we present the results of our calculations of dynamic and equilibrium properties, and finally, in section 5 we summarize the main results.

2. Potential Energy Surfaces

Since we are aiming to study the dynamics of large size atomic aggregates, we must formulate analytical potential functions. As mentioned earlier, ab initio calculations suggest that the electrostatic forces prevail in the interactions of Mg^+ with Ar.[19] Therefore, we adopt an electrostatic model. The potential is written as[8]

$$V_{tot} = \sum_{k=2}^{n+1} V_n^+(1,k) + \sum_{j=2}^{n} \sum_{k=j+1}^{n+1} V_{nn}(j,k) \quad (1)$$

The first sum describes the interactions of the Mg ion (labeled as atom 1) with the atoms of argon (labeled as atoms 2, 3, ..., $n + 1$). The second term in eq 1 denotes the interactions among argon atoms.

The first term is developed as

$$V_n^+(1,k) = V_0(r_{1k}) + V_{dis}(r_{1k}) - \frac{1}{2}a_k E_k^2 \Phi(r_{1k}) - \frac{1}{2}a_1\vec{E}_{1k}\vec{E}_1 + \frac{a_1 a_k E_1 E_k}{r_{1k}^3}[\hat{E}_1\hat{E}_k - 3(\hat{E}_1\hat{r}_{1k})(\hat{E}_k\hat{r}_{1k})] \quad (2)$$

where $\vec{r}_j$ is the position vector of atom j in a space fixed cartesian coordinate system, $\vec{r}_{jk} = \vec{r}_j - \vec{r}_k$, and its norm $r_{jk} = |\vec{r}_j - \vec{r}_k|$; a_1 is the polarizability of the magnesium cation; $a_k = a_{Ar}$ is the polarizability of the argon atom k, $k = 2, 3, ..., n + 1$; $\vec{E}_k$ is the intensity of the electric field at the position of atom k,

$$\vec{E}_k = \frac{Q}{r_{k1}^2}(1 - \delta_{k1})\hat{r}_{k1} + \sum_{l=1, l\neq k}^{n+1} \frac{a_l E_l}{r_{kl}^3}[3(\hat{r}_{kl}\hat{E}_l)\hat{r}_{kl} - \hat{E}_l] \quad (3)$$

(where Q is the electric charge on atom 1, and δ_{k1} is Kronecker's delta function); $\vec{E}_{1k}$ is the contribution to the intensity of the electric field at the position of the ion which is due to the dipole moment of atom k; $\hat{E}_k$, $\hat{r}_{jk}$ are the unit vectors in the directions of the intensity of the electric field on the atom k and of the position of atom k relative to atom j, respectively; and $\Phi(r_{1k})$ is a switching function which effects a smooth interpolation between short-range and charge−induced dipole interactions.

The first two terms in eq 2 denote the repulsive and the dispersion potentials, respectively. Both these terms are described with a diatomic Morse type function

$$V_0(r) + V_{dis}(r) = Ae^{2B(1-r/D)} - 2Ce^{B(1-r/D)} \quad (4)$$

The third term in eq 2 is the charge−induced dipole interaction, the fourth term describes the effect of all other atoms on the ion, and the fifth term is due to the induced dipole− induced dipole interactions.

$A = 2.262 107 16 \times 10^5$	$c_{10} = 0.346 027 94$
$a = 10.778 747 43$	$d = 1.36$
$b = -1.812 20 04$	$\epsilon = 0.284 62$ kcal/mol
$c_6 = 1.107 851 36$	$r_0 = 7.098 756 333$ a_0
$c_8 = 0.560 724 59$	

The part of the potential which yields the Ar−Ar interactions is written as

$$V_{nn}(j,k) = V(r_{jk}) + \frac{a_j a_k E_j E_k}{r_{jk}^3}[\hat{E}_j\hat{E}_k - 3(\hat{E}_j\hat{r}_{jk})(\hat{E}_k\hat{r}_{jk})] \quad (5)$$

This is the sum of a potential valid for a free argon dimer and an electrostatic induced dipole−induced dipole interaction. $V(r_{jk})$ is given by an empirical function proposed by Aziz and Slaman,[24]

$$V(x) = \epsilon\left(Ae^{-ax+bx^2} - \begin{cases} e^{-((d/x)-1)^2} & x < d \\ 1 & x \geq d \end{cases}\right)\left[\frac{c_6}{x^6} + \frac{c_8}{x^8} + \frac{c_{10}}{x^{10}}\right]) \quad (6)$$

where

$$x = r/r_0$$

For the completeness of this paper the values of the parameters in the above potential are displayed in Table 1. The polarizabilities of the atoms are $a_{Ar} = 11.13$ a_0^3,[19] $a_{Mg^+} = 37.11$ a_0^3,[19] and $a_{Mg^{2+}} = 0.6$ a_0^3.[22]

It should be noted that eq 1 is not a pairwise additive function. Many-body interactions are introduced through the electrostatic terms. The induced dipole moment on atom k depends on the positions of all other atoms. To fit the parameters that appear in the above functional form, we separately study the small clusters of Mg^+ and Mg^{2+}.

2.1. Potential Energy Surface of Mg^+Ar_n. Bauschlicher and co-workers[19] employed the self-consistent-field method and the modified coupled-pair functional approach (SCF MCPF) for the electron correlation to calculate the binding energies and geometries of a number of metal ions with inert gases. For Mg^+ they determined the energy and geometry of the minima with one and two argon atoms in their electronic ground states, $^2\Sigma^+$ and $^2A_1$, respectively. An extended basis set was used for magnesium that consist of (21s16p8d6f) and contracted to [7s7p4d3f], and for argon (17s12p6d4f)/[6s5p3d1f].

The ab initio results for Mg^+Ar were employed to fit the parameters of the Morse type potential (eq 4), and these are the minimum energy, -3.25 kcal/mol, the harmonic frequency, 92 cm^{-1}, and the equilibrium bond length, $r_m = 5.47$ a_0. The zero of the total energy is defined with all atoms separated at their electronic ground state. In the Morse type function we fix the parameter D to be equal to the equilibrium bond length, r_m, and the other parameters are fitted such that the total potential of the diatomic (eq 2) exactly reproduces the ab initio results. The following switching function $\Phi(r)$ (eq 2) was chosen:

$$\Phi(r) = \tanh\left(\frac{r - E}{F}\right) \quad (7)$$

We adjust the parameters E and F in such a way that the potential of Mg^+Ar_2 reproduces the energy and geometry of the minimum (an isosceles triangle) obtained from the ab initio calculations of Partridge et al.[19] These values are $E_0 = -6.2$

TABLE 2: Fitted Values of the Parameters Used in the Morse Type Potential and Switching Functions (Eqs 4, 7, 8) ($r_m = D$ Is the Equilibrium Bond Length of Mg^+Ar)

	A/hartrees	B/a_0^{-1}	C/hartrees	D/a_0	E	F
Mg^+Ar	0.007 604 54	4.157 812 15	0.002 264 53	5.47 (r_m)	4.5	0.4
$Mg^{2+}Ar$	0.035 077 68	3.944 470 24	$C = A$	4.478 580 86	7.0	0.0

TABLE 3: Minima of $Mg^{2+}Ar_n$ Clusters[a]

n	r (a_0)	E_{SCF}	$E_{SCF-MP2}$	$E_{SCF-MP2}^\infty$	E_0
1	4.44	−725.671 989	−726.036 925	−725.992 666	−27.772
	(4.44)				(−27.772)
2	4.48	−1252.516 465	−1253.117 368	−1253.032 757	−53.093
	(4.51)				(−52.23)
3	4.53	−1779.353 432	−1780.190 837	−1780.072 847	−74.038
	(4.57)				(−73.51)

[a] E_{SCF} is the electronic ground state energy at the SCF level, $E_{SCF-MP2}$ is the energy at the MP2 level, and $E_{SCF-MP2}^\infty$ is the electronic energy with the atoms separated at large distances. Energies are in Hartrees. E_0 is the binding energy of the cluster in kcal/mol, with the zero of the energy defined with all atoms separated in their electronic ground states. The numbers in parentheses are calculated values with the analytical potential.
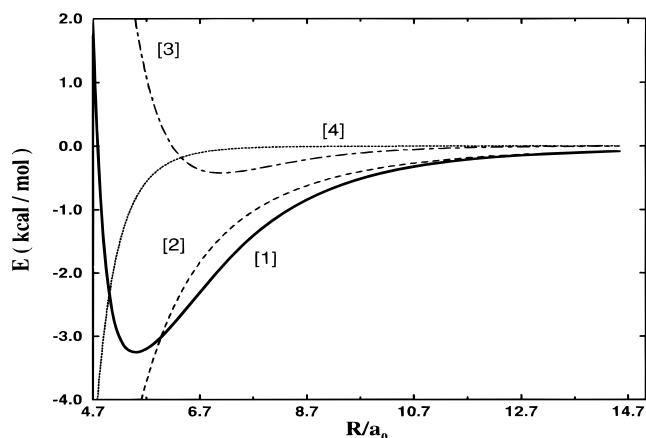
Figure 1. Fitted potential curve for the electronic ground state ($^2\Sigma$) of Mg^+Ar. The continuous line, [1], is the total potential given by eq 2. The dashed line, [2], describes the charge−induced dipole interaction, the dotted line, [4], is the last two terms of eq 2, and the double dashed line, [3], is the Morse type potential.

kcal/mol; the equilibrium geometry is at the Mg^+Ar bond length $r = 5.56$ a_0, and the angle between the two Mg^+Ar bonds is equal to 82.5°. The fitted values of the parameters, A, B, C, D, E, and F, are tabulated in Table 2.

Figure 1 shows the potential curve for Mg^+Ar. The continuous line labeled with [1] is the total potential, [2] denotes the charge−induced dipole interaction term, [3] is the Morse type potential, and [4] is the last two terms in eq 2.

The analytical function for the triatomic system Mg^+Ar_2 gives a minimum of −6.06 kcal/mol, at $r = 5.62$ a_0, and the angle between the two bond lengths is 77°. This potential function is used to study larger clusters.

2.2. Potential Energy Surface of $Mg^{2+}Ar_n$. We have used the package of programs GAMESS[25] to calculate the geometries and energies of the most stable structures of $Mg^{2+}Ar_n$ for $n = $ 1, 2, and 3. SCF type calculations were performed, and the electron correlation energy was treated at the MP2 level. The basis set which we used for Mg is (12s8p2d)/[8s5p2d] (triple-ζ valence plus polarization, TZV+P), and for Ar (13s10p2d)/ [8s5p2d] (TZV+P). The MP2 calculations were done with no frozen core orbitals.

Table 3 presents the electronic energies for $Mg^{2+}Ar_n$, $n = 1$, 2, and 3. A linear geometry ($D_{\infty h}$) was found for the triatomic
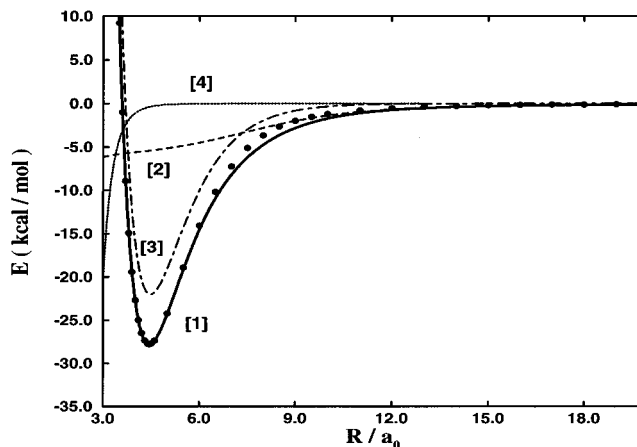
Figure 2. Fitted potential curve for the electronic ground state ($^1\Sigma$) of $Mg^{2+}Ar$. The continuous line, [1], is the total potential given by eq 2. The dashed line, [2], describes the charge−induced dipole interaction, the dotted line, [4], is the last two terms in eq 2, and the double dashed line, [3], is the Morse type potential. The dots along the total potential curve denote the ab initio points.

TABLE 4: Comparison of SCF-MP2 and Analytical Function Binding Energies for Configurations Far from the Equilibrium Point of the $Mg^{2+}Ar_2$ Cluster (r_3 is the Distance between the Two Argon Atoms)

r_1	4.5	4.74	5.87	5.19	5.87	6.64
r_2	4.5	4.74	5.87	7.50	5.19	6.24
r_3	9.0	8.60	8.60	12.67	7.60	10.10
ab initio	−50.10	−50.59	−29.29	−30.56	−23.81	−20.74
analytical	−49.74	−50.61	−30.30	−31.54	−25.07	−22.17
r_1	6.64	5.39	5.66	6.09	5.19	5.45
r_2	6.64	4.41	3.86	4.46	5.87	6.64
r_3	10.60	9.60	8.60	8.60	8.60	9.00
ab initio	−18.10	−46.16	−32.94	−39.48	−35.60	−27.87
analytical	−19.72	−46.09	−32.49	−40.04	−36.56	−28.95

system, and a planar minimum of D_{3h} symmetry was found for the tetraatomic with the magnesium ion in the center of the triangle.

In the fitting process of $Mg^{2+}Ar_n$ the switching function $\Phi(r)$ (eq 2) was chosen as

$$\Phi(r) = 1 - \exp[-(r/E)^4] \qquad (8)$$

As in the case of the monocation, we have used the ab initio results to fit the parameters in the Morse type potential and switching function. Table 2 exhibits their values. Figure 2 shows the total potential curve [1] and the contributing terms. As before [2] denotes the charge−induced dipole term, [3] the Morse function for the short range interactions, and [4] the last two terms in eq 2.

The parameters in the switching function (eq 8) were chosen so as to reproduce the energy and geometry of the triatomic. The values in the parentheses shown in Table 3 are those that are calculated with the analytical function. In Table 4 we compare the energies for some other configurations of the triatomic system far from the minimum. As can be seen, the energies predicted from the analytical potential function are in satisfactory agreement with the ab initio calculations.

3. Minimum Energy Structures

Generally, we are interested in finding not only the absolute minima of the small size clusters but also a number of relative

minima and saddle points that separate them. The knowledge of the stationary points of a dynamical system provides a zero-order approximation to the dynamical properties of the system.[26]

In this work, we apply the same minimization techniques used in previous studies on water clusters.[3,4] These are the Newton–Raphson method and the method of integration of friction equations. The Newton–Raphson technique is an iterative method to locate the roots of the nonlinear algebraic equations,

$$\vec{f}_i = 0 \quad i = 1, 2, ..., n + 1 \tag{9}$$

where $\vec{f}_i$ are the forces exerted on the atom i

$$\vec{f}_i = -\frac{\partial V(\vec{r})}{\partial \vec{r}_i}, \quad i = 1, 2, ..., n + 1 \tag{10}$$

The friction method requires the integration of the first order differential equations,

$$\dot{\vec{r}} = \frac{d\vec{r}}{dt} = -\kappa \frac{\partial V(\vec{r})}{\partial \vec{r}_i} \tag{11}$$

where κ^{-1} is the friction coefficient. We use standard integrators[27] to solve the above system of differential equations.

Although the Newton–Raphson method converges quadratically, very often it diverges because of a bad starting point. We have found that the combination of the above two techniques guarantees convergence. The way we apply it is to locate first the stationary point with the friction method by requiring low accuracy. Then, we find the root of eq 9 with the Newton–Raphson method and with higher precision. The stability properties of the stationary point are determined by linearizing the Hamilton equations of motion and, then, diagonalizing the matrix of the second derivatives of the Hamiltonian.[26] If all eigenvalues are pairs of imaginary numbers, $\pm i\mu$, the stationary point is stable (minimum). If there are k pairs of real eigenvalues, $\pm\mu$, the stationary point is a saddle point of kth order.

We have investigated and compared other minimization techniques, such as the conjugate gradient and the variable metric methods, and the results will be presented in another publication.[28]

In the search for different minima of low energy we select starting points for the minimization procedure using several algorithms. We employ a Monte Carlo method for obtaining random positions of the atoms, or we construct initial configurations systematically using a building up principle. Finally, to find minima which are dynamically connected, we integrate the classical equations of motion and at regular time intervals we store the phase space points that are visited. These points provide initial conditions for the minimization algorithms. New regions of phase space are explored when the total energy of the cluster is increased.

In the application of the minimization techniques the PVM (parallel virtual machine) package of programs[29] were very helpful. They enabled us to use simultaneously several distributed computers.[6]

3.1. Mg$^+$Ar$_n$, $n = 3$–14. The lowest energy minima found for the clusters of Mg$^+$Ar$_n$ and for $n = 3$–14 are shown in Figure 3. In Table 5 we tabulate the total energies (E) and the energy per argon atom (E/n).

The geometries of the absolute minima of the first clusters $n = 3, 4, 5,$ and 6 are a trigonal pyramid of C_{3v} symmetry, two triangular pyramids which share a common side, the previous structure with one more Ar atom in the middle of a triangle formed by a Mg ion and two argon atoms, and a regular
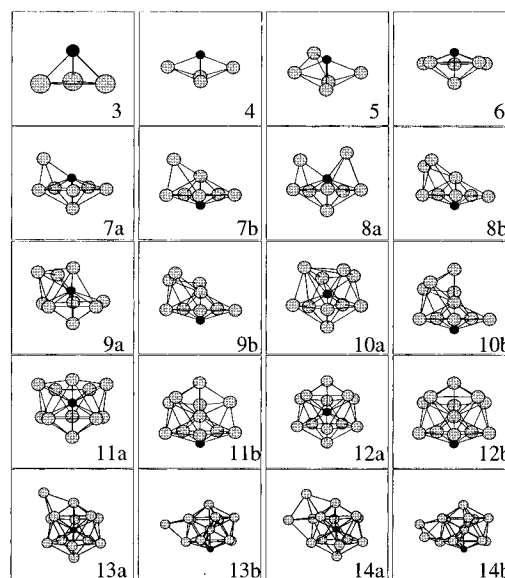
Figure 3. Minimum energy structures for the clusters Mg$^+$Ar$_n$, $n = 3$–14. For $n > 6$ two isomers are shown, one with the Mg ion in the interior of the cluster *(a)* and one with the ion on the surface *(b)*.

TABLE 5: Total Energies, E, Energy per Atom, and Energy per Argon Atom of the Minima of Mg$^+$Ar$_n$ Clusters^a

n	$-E$	$-E/n + 1$	$-E/n$	type
3	8.692	2.173	2.897	
4	10.520	2.104	2.630	
5	12.088	2.015	2.418	
6	13.864	1.980	2.311	
7	15.080	1.885	2.154	*a*
	15.072	1.884	2.153	*b*
8	16.567	1.840	2.071	*a*
	16.532	1.837	2.067	*b*
9	18.029	1.802	2.003	*a*
	18.013	1.801	2.001	*b*
10	19.522	1.775	1.952	*a*
	19.730	1.794	1.973	*b*
11	21.113	1.759	1.919	*a*
	21.530	1.794	1.957	*b*
12	23.056	1.774	1.921	*a*
	23.589	1.815	1.966	*b*
13	24.125	1.723	1.856	*a*
	24.744	1.767	1.903	*b*
14	25.440	1.696	1.817	*a*
	26.120	1.741	1.866	*b*

^{a} Isomers *(a)* are those with the magnesium ion in the interior, and isomers *(b)* with the ion on the surface. Energies are in kcal/mol. The zero of the energy is defined with all atoms separated in their electronic ground states.

pentagon with the sixth argon atom in the middle of one side of the pentagon and the magnesium on the opposite side (C_{5v}).

By adding more Ar atoms, we generate two series of minima with small differences in the energies of the isomers: one with the extra atoms on the same side as magnesium, thus closing the cation in the interior of the cluster, and the other with the metal atom always on the surface. The first type of minima, which correspond to clusters with a solvated magnesium ion, are denoted with the letter *(a)* and the second type, with a nonsolvated cation, with the letter *(b)*.

The energy differences between the two isomers *(a)* and *(b)* are small, and as can be seen from Table 5, this difference increases for the large clusters. The geometries of the Mg$^+$-Ar$_{12}$ isomers are an icosahedral structure of I_h symmetry for *(a)* and C_{5v} symmetry for *(b)*. With $n = 12$ the first shell is completed, and larger clusters are formed by filling the second shell. We find that in the case of the Mg$^+$Ar$_{12}$- *(b)* isomer the
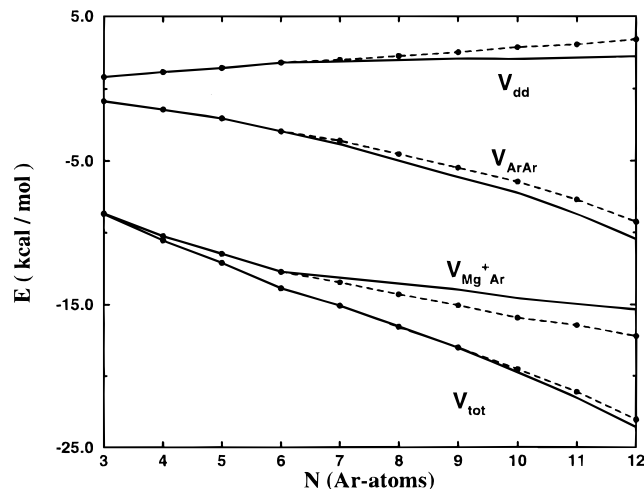
Figure 4. Plots of the total energy (V_{tot}), ion−induced dipole interaction (V_{Mg^+Ar}), Ar−Ar interaction (V_{ArAr}), given by eq 6, and the induced dipole−induced dipole interactions (V_{dd}), among argon atoms, as functions of the size of the cluster.

extra Ar atoms prefer to stay on the same side as the other argon atoms and not on the side of magnesium.

Looking at Table 5, we make the following interesting remarks. The binding energy per argon atom decreases with increasing cluster size, but for $n = 12$ we can see a small increase. This is an indication of the extra stability of Mg^+Ar_{12}.

For $n = 10$ and larger clusters the *(b)* isomers have lower energy than the *(a)*, reversing the trend observed in the smaller clusters for which the *(a)* structures were the absolute minima. In other words, energetically, Mg^+ prefers to remain nonsolvated in the large clusters.

This behavior can be elucidated with the analysis of the total energy into the contributing terms. Figure 4 shows the total energy, V_{tot}, the ion−induced dipole interaction, V_{Mg^+Ar}, the Ar−Ar interaction given by eq 6, V_{ArAr}, and the induced dipole−induced dipole interactions, V_{dd}, among argon atoms, as functions of the size of the cluster. Dashed lines denote the series *(a)*, and continuous lines the series *(b)*. For the small clusters (up to $n = 6$) the repulsive term V_{dd} balances the attractive term V_{ArAr}, as can be seen from the approximately symmetric split of these two curves in Figure 4. Therefore, the stability of the cluster is determined mainly by the attractive V_{Mg^+Ar} term.

The symmetric split of the two contributing terms of the Ar−Ar interaction is destroyed for larger clusters, and both terms V_{dd} and V_{ArAr} favor the nonsolvated magnesium−argon clusters. For the isomers *(b)* the repulsion of the induced dipole−induced dipole interaction is less because of the better orientation of the dipole moments, and also the Ar−Ar attraction becomes more efficient. Contrary to that, the ion−induced dipole interaction favors a solvated magnesium. The balance of the terms V_{Mg^+Ar}, V_{ArAr}, and V_{dd} determines the stability of the cluster. For example, for Mg^+Ar_{12} the numerical values for the above three terms are -17.219, -9.242, and $+3.405$ kcal/mol for isomer *(a)* and -15.365, -10.464, and $+2.239$ kcal/mol for isomer *(b)*.

We may conclude that the icosahedral structure of Mg^+Ar_{12} has two isomers, one with the metal atom in the center and the other with the ion on the surface. Our potential predicts as a lower energy minimum the one with Mg on the surface. However, taking into account the small difference in energy between these two isomers, it is difficult to claim that this is a final conclusion. Ab initio calculations or spectroscopic experiments are needed.
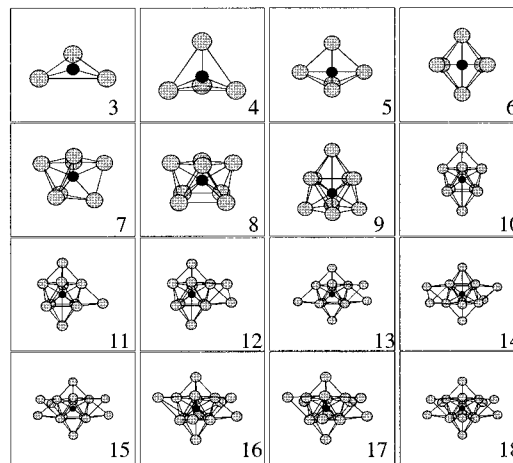
Figure 5. Minimum energy structures for the clusters $Mg^{2+}Ar_n$, $n = 3-18$.

TABLE 6: Total Energies, E, Energy per Atom, and Energy per Argon Atom of the Minima of $Mg^{2+}Ar_n$ Clusters[a]

n	$-E$	$-E/n + 1$	$-E/n$
3	73.506	18.377	24.502
4	92.526	18.505	23.132
5	107.877	17.980	21.575
6	123.313	17.616	20.552
7	129.156	16.144	18.450
8	135.887	15.098	16.986
9	139.202	13.920	15.476
10	142.320	12.938	14.232
11	144.559	12.047	13.142
12	146.881	11.298	12.240
13	149.043	10.646	11.465
14	151.303	10.087	10.807
15	153.484	9.593	10.232
16	155.724	9.160	9.733
17	157.848	8.769	9.285
18	160.038	8.423	8.891

[a] Energies are in kcal/mol. The zero of the energy is defined with all atoms separated in their electronic ground states.

We have made a harmonic frequency analysis for all minima that we have located. For Mg^+Ar_6 the highest frequency is about 80 cm^{-1}, and for the clusters of type *(a)* this value decreases as the size increases. On the contrary, for the type *(b)* structures the highest frequency increases, reaching a value of 160 cm^{-1} at $n = 12$. The normal coordinate that corresponds to this eigenfrequency describes mainly vibrations of the metal ion and of the argon atom which is in the center of the icosahedral structure. In the following sections we argue that this is a characteristic which distinguishes the two isomers.

3.2. $Mg^{2+}Ar_n$, $n = 3-18$. We have seen that the binding energy of $Mg^{2+}Ar$ is almost 1 order of magnitude larger than that of Mg^+Ar and that the equilibrium bond length of the former is smaller. Consequently, the induced dipole moments on the argon atoms are larger and the minimum energy geometries of $Mg^{2+}Ar_n$ clusters are expected to be markedly different from those of the monocation.

Figure 5 shows the geometries for $n = 3-18$, and Table 6 tabulates their energies. For $n = 3$ a planar triangular D_{3h} geometry is found with the Mg ion in the center, for $n = 4$ a regular tetrahedron (T_d) is predicted, and for $n = 5$ a C_{2v} symmetry structure is located. A regular octahedron is the geometry of $Mg^{2+}Ar_6$ (O_h). Addition of one more Ar atom destroys this high symmetry.

It is worth mentioning that we have carried out SCF type calculations for $n = 4$, 5, and 6 with a smaller basis set than

Potential Functions of Mg^{m+}Ar$_n$ (m = 1, 2; n = 1−18) Clusters

J. Phys. Chem., Vol. 100, No. 10, 1996 **3905**
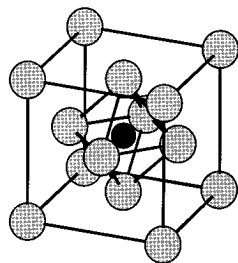
Figure 6. Fcc type minimum of Mg^{2+}Ar$_{14}$ with energy equal to −145.016 kcal/mol.
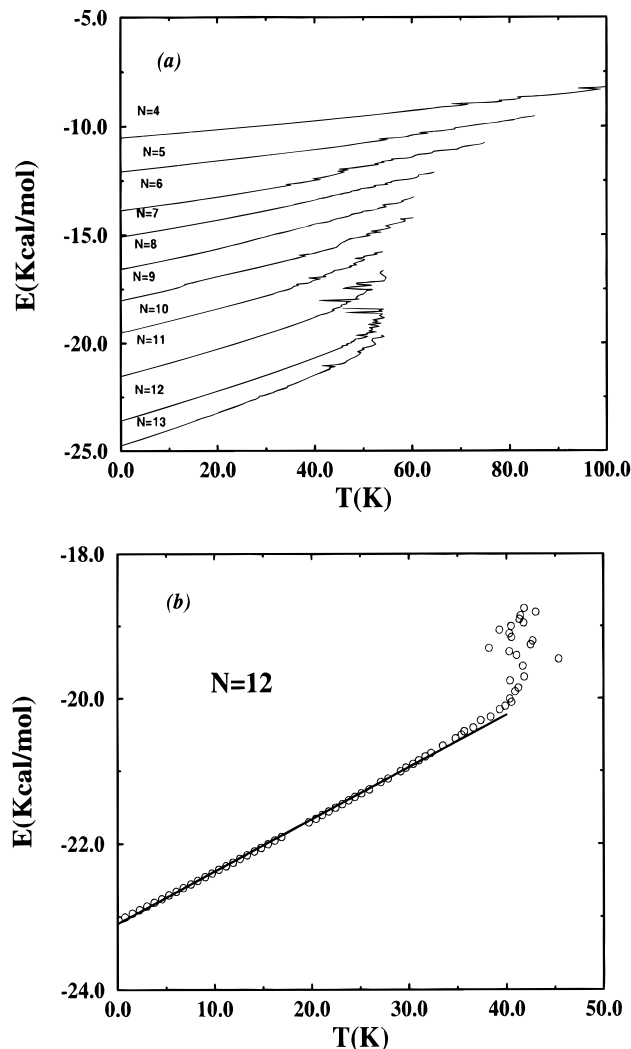
Figure 7. (a) Caloric curves of Mg$^+$Ar$_n$ for n = 4−13. (b) The caloric curve of the Mg$^+$Ar$_{12}$(a) isomer.

Figure 8. Bond length root mean square fluctuations, $\delta(T)$, of all distances for the clusters Mg$^+$Ar$_n$ with n = 7−13.
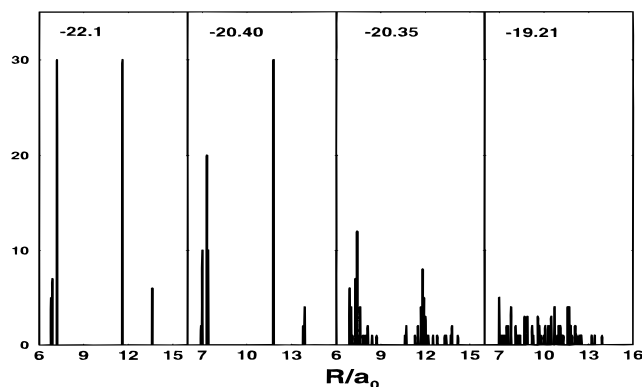
Figure 9. Time average distributions of all distances of Mg$^+$Ar$_{12}$(a) for four different energies. Energies are in kcal/mol.

that used before, and we found minima of the same symmetry as those given by the model potential.

For Mg^{2+}Ar$_8$ a square antiprism is formed as the lowest energy minimum. The next two clusters in the series are obtained by putting one argon atom above and one below and in the center of each square, respectively. Larger clusters are constructed by adding argon atoms on the sides of Mg^{2+}Ar$_{10}$, as shown in Figure 5. The series is completed with the Mg^{2+}-Ar$_{18}$ cluster. For all these complexes we have not located a minimum with the metal atom on the surface.

If we adopt the assumption that magic numbers correspond to the clusters of high symmetry or result after the completion of a shell of atoms, then we would expect that the second peak in the mass spectrum would be for n = 18. This is not in agreement with the experimental observation which shows a

broad peak at n = 14. Such a minimum might result by putting Ar atoms of the second shell at the centers of the sides of the regular octahedral Mg^{2+}Ar$_6$, thus obtaining a fcc type geometry (Figure 6). We have located this minimum, but it is of higher energy (−145.016 kcal/mol).

The geometries which we find for the clusters with n>6 are the result of the electrostatic model. However, we must point out that the ab initio calculations have shown a significant charge transfer, and that means that the electrostatic potential may not be very accurate for the larger clusters.

In conclusion, we may say that the energetics of Mg^{2+}Ar$_n$ aggregates favor solvated structures as a result of the strong ion−induced dipole interaction.

4. Dynamic Properties

The stationary points of the potential energy surface provide a zero-order approximation to the dynamics of the cluster, since for small excitation energies a harmonic approximation of the pes is satisfactory. Thus, the motions around the stationary points are known (both classically and quantum mechanically). However, in dealing with highly anharmonic and strongly coupled potential functions, it is necessary to study the full dynamics as the excitation of the system becomes appreciable. In particular, we are interested in finding out the energy at which the system ceases to explore only the minimum well and the atoms start moving erratically through an extended phase space. In other words, the trajectory of the cluster at some particular energy overcomes the potential barrier(s) and visits other minima
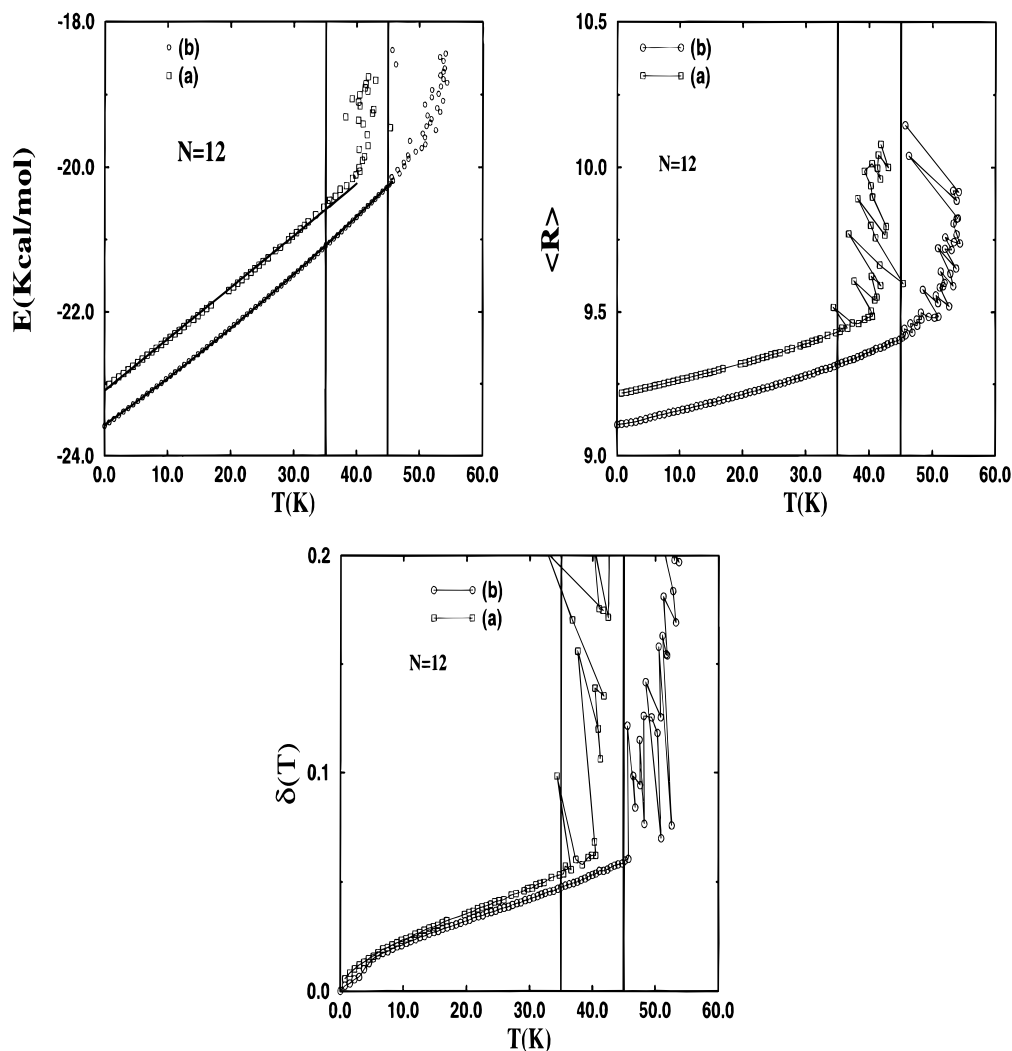
Figure 10. Comparison of the caloric curves, the average Mg−Ar distances, and their root mean square fluctuations, $\delta(T)$, of the isomers *(a)* and *(b)* of Mg^+Ar_{12}.

of the pes in which it can be trapped for appreciable time intervals. Numerous studies have been done for investigating these transitions, which are now customarily referred to as phase transitions from solid-like to liquid-like. Most of these studies have been done for Ar_n clusters with pair additive Lennard-Jones potentials.[30,31]

Equilibrium properties at some particular energy are evaluated using either Monte Carlo or molecular dynamics techniques. For relatively small size systems, like the clusters we are studying, molecular dynamics methods are more efficient. The latter require the solution of the classical equations of motion, and in our case we integrate the Hamilton equations of motion.

The atomic aggregate is described in a space-fixed Cartesian coordinate system. A variable order, variable time step algorithm is used to integrate Hamilton's equations.[27] The properties that we are interested in are the same as those computed in our previous work on water clusters.[3−6] These are average values of the distances Mg^{m+}−Ar and Ar−Ar and root mean square fluctuations of the distances from the average values, δ,

$$\delta = \frac{2}{n(n+1)}\sum_{i=1}^{n}\sum_{j=i+1}^{n+1}\frac{[\langle r_{ij}^2\rangle_t - \langle r_{ij}\rangle_t^2]^{(1/2)}}{\langle r_{ij}\rangle_t} \qquad (12)$$

where $\langle\ \rangle_t$ denotes time average values. Equation 12 defines

the root mean square fluctuations of all distances. Similar equations are valid for the fluctuations of the $Mg^{m+}Ar$ and ArAr bond lengths separately.

We also compute the average kinetic energy, and using the equipartition law, we estimate a temperature for the cluster, caloric curves, that is the total energy as a function of the temperature, velocity autocorrelation functions, $C(t)$,

$$C(t) = \frac{\langle \vec{v}(t_0 + t)\cdot\vec{v}(t_0)\rangle_t}{\langle \vec{v}^2(t_0)\rangle_t} \qquad (13)$$

and from it power spectra, as well as radial distribution functions.

To obtain the average values, we integrate one trajectory at total energy E, for time intervals which vary between 500 ps and 1 ns. The energy of the system is increased by scaling the momenta, and then we leave the system to relax by integrating the new trajectory for times of 100−200 ps before we start selecting points for the evaluation of the average values. To test for convergence, in a few runs we compare the results by doubling the integration time of the trajectory and by increasing the energy with smaller energy steps. Negligible differences were found in these tests.

4.1. Mg^+Ar_n. We first examine possible phase transitions for the clusters of the magnesium monocation. Signatures of such events may be seen in the caloric curves and in plots of the root mean square bond length fluctuations. Figure 7a shows

Potential Functions of $Mg^{m+}Ar_n$ ($m = 1, 2$; $n = 1-18$) Clusters

J. Phys. Chem., Vol. 100, No. 10, 1996 **3907**
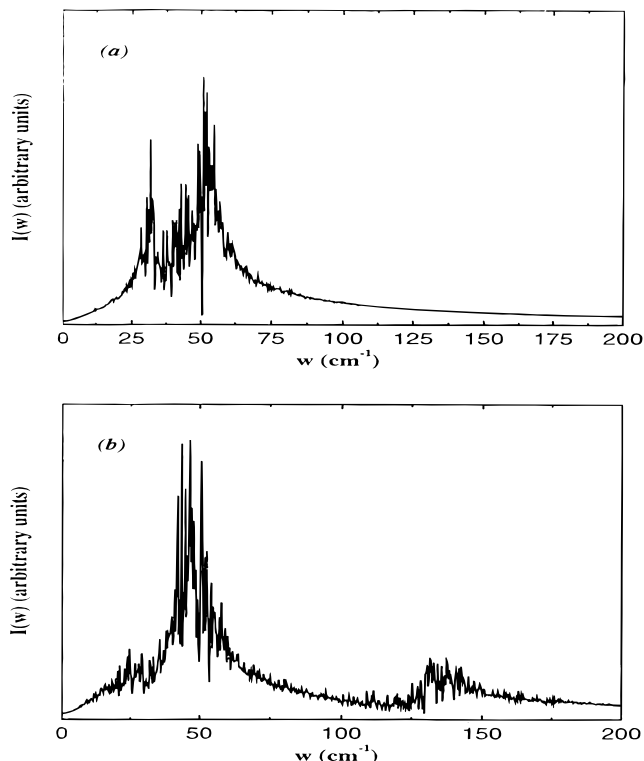
Figure 11. Power spectra of Mg^+Ar_{12} at 35 K for the isomer *(a)* and 45 K for the isomer *(b)*. For the latter, the characteristic band at 130 cm^{-1} that discerns this isomer can be seen (see text).

the caloric curves for the clusters with $n = 4-13$. Figure 7b presents the caloric curve of $Mg^+Ar_{12}(a)$ for a better inspection.

As is well-known, the temperature at the phase transition is better estimated in plots of the root mean square fluctuations of the distances, and Figure 8 shows the results of $Mg^+(b)$ clusters for $n = 7-13$. At the temperature at which the system starts exploring large regions of phase space, the δ function exceeds the value of 0.1 (Lindemman's criterion).[32]

From Figure 8 we can see that the icosahedron of Mg^+Ar_{12} is the most stable cluster. Its transition temperature is about 45 K. The stability of the cluster is further examined by computing distributions of the average distances at different energies. For example, Figure 9 shows such distributions for the $Mg^+Ar_{12}(a)$ at four different energies. At low energies where the cluster remains in the potential well the histograms reveal the distances of Mg−Ar and Ar−Ar encountered in the icosahedron. The plot at the energy −20.35 kcal/mol, which corresponds to the transition region in the caloric curve, shows that the distributions are broader but still around the peak values found at lower energies. Finally, at very high energies the distributions tend to become uniform.

We have found two series of minima for Mg^+Ar_n, $n > 7$, clusters: one with the Mg ion inside and the other with the ion on the surface of the cluster. Now, we address the question of which of these two isomers is dynamically more stable for $n = 12$. In Figure 10 we compare the caloric curves, the average Mg−Ar distances, and their root mean square fluctuations, $\delta(T)$. We estimate the transition temperature to be 35 K for the isomer *(a)* and 45 K for the isomer *(b)*.

Figure 11 shows the power spectra obtained from the Mg ion velocity autocorrelation function of the two Mg^+Ar_{12} isomers at temperatures that correspond to the phase transition. The characteristic band at 130 cm^{-1} is red-shifted from the harmonic frequency (160 cm^{-1}). This feature can be used to discern the isomer *(b)* from isomer *(a)*. Similar plots at lower energies show narrower bands.

From the above we may conclude that the icosahedral structures of Mg^+Ar_{12} are stable dynamically as well as energetically. Between the two isomers *(a)* and *(b)* the one with Mg^+ on the surface is the most stable.

4.2. $Mg^{2+}Ar_n$. A dynamic analysis of Mg^{2+} clusters has been carried out for $n = 5-7$. Figure 12 shows the root mean square fluctuations of all distances for $n = 5$, 6, and 7. We can see an almost linear increase for $n = 6$ up to 600 K. It is interesting to note that for $n = 7$ a rather low transition energy is observed (20 K). This is due to the asymmetric geometry of this cluster, which makes the movements of Ar atoms easy.

Figure 13 shows average distances as functions of the temperature for the clusters $n = 5$, 6, and 7. The mobility of Ar atoms in the clusters $Mg^{2+}Ar_5$ and $Mg^{2+}Ar_7$ can be seen. In contrast, $Mg^{2+}Ar_6$ shows a linear dependence with the temperature up to 600 K. For all these energies the octahedral
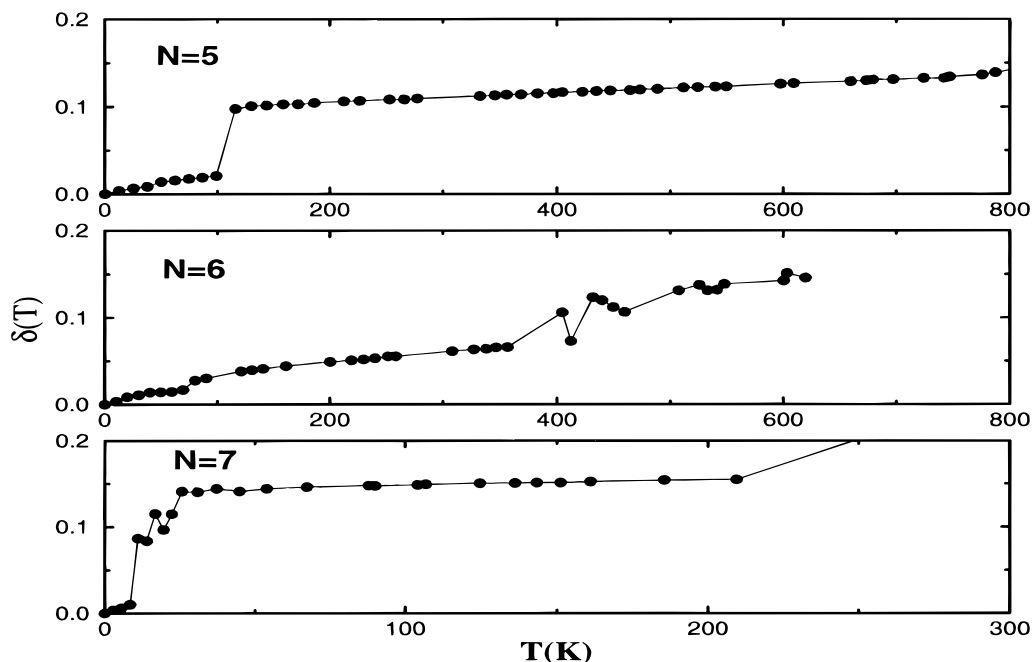
Figure 12. Root mean square fluctuations, $\delta(T)$, of $Mg^{2+}Ar$ distances for the clusters $Mg^{2+}Ar_n$ with $n = 5-7$.
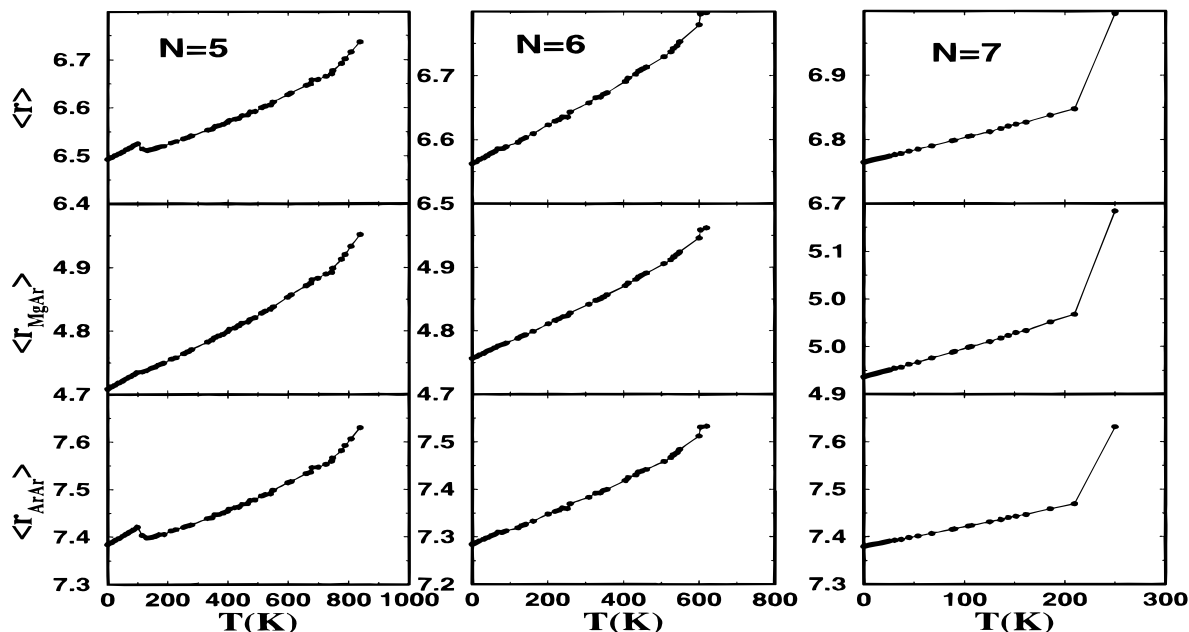
Figure 13. Average values of the distances of $Mg^{2+}Ar_n$ clusters. $\langle r \rangle$ is the average value of all distances in the cluster.

geometry of the cluster is not destroyed on the average, and this is considered as an indication of the extra stability of this conformer.

5. Discussion and Conclusions

Using ab initio calculations for the small clusters of Mg^{m+}-Ar_n, $m = 1$, and 2, we have constructed analytical potential functions based on the electrostatic expansion of charge−induced dipole and induced dipole−induced dipole interactions. Minimum energy geometries and equilibrium properties have been investigated with molecular dynamics techniques.

The main results are as follows.

(1) The lowest minimum energy structures of Mg^+Ar_n, $n = 1−14$ are similar to those of Ar_{n+1} clusters, with a regular icosahedral geometry for the Mg^+Ar_{12} cluster, and this despite the much stronger attraction of Ar atoms by the Mg ion. However, we have found for $n > 6$ two energetically nearly equivalent isomers. Isomer *(a)* has Mg in the center, and isomer *(b)* has the ion on the surface and an argon atom in the center. Our potential function predicts that isomer *(b)* is more stable in absolute energy for $n > 9$.

The coexistence of solvated and nonsolvated isomers for heterogeneous clusters has been cited in the literature already. A case similar to ours is that of the transition metal V^+Ar_n[33] clusters. The authors have made an analysis of the potential function terms to investigate when the metal atom is attached to the surface of the aggregate.

However, a more interesting case is that of the neutral clusters of SF_6Rg_n[34] for Rg = Ar and Kr. Isomers with the rare gas (Rg) atoms covering the molecule and isomers with the Rg atoms stacked on one face of SF_6 were found. The investigators tried to rationalize these tendencies by analyzing the total potential into two contributing terms. They showed that the competition between the pulling of Rg−SF_6 anisotropy of the potential and the tendency for the rare gas atoms to achieve the best packing geometries results in the two types of isomers, solvated and nonsolvated. What is striking, as far as the argon clusters are concerned, is the similarities in the geometries of the lowest minima with those of Mg^+Ar_n aggregates that involve a spherically symmetric solute atom. For example, the cluster with six argon atoms forms a regular pentagon, whereas for n

= 12 the argon atoms form the icosahedral structure with one of the protruding F atoms as a vertex. Thus, the latter structure corresponds to the *(b)* type isomer that we found for the magnesium cation.

(2) Caloric curves, radial distributions, distance mean square fluctuations, and power spectra point out that the icosahedron of Mg^+Ar_{12}, for both solvated and nonsolvated isomers, is more stable with respect to the temperature at which a phase transition is observed compared to the smaller and larger clusters. The same indicators show that isomer *(b)* has a transition temperature at about 45 K, and isomer *(a)* at 35 K.

(3) Analysis of the harmonic frequencies reveals that clusters of type *(b)* have a distinguishable large frequency compared to clusters *(a)*. For Mg^+Ar_{12} isomers the maximum harmonic frequency for *(a)* is about 50 cm^{-1} and for *(b)* 160 cm^{-1}.

(4) Ab initio calculations at the SCF-MP2 level have been performed for $Mg^{2+}Ar_n$, $n = 1$, 2, and 3. Based on these calculations an electrostatic potential function was constructed to study larger clusters.

(5) For the minimum of $Mg^{2+}Ar_6$ a regular octahedron of O_h symmetry is found. The $n = 8$ atomic aggregate has a square antiprism geometry, and the $n = 10$, a capped structure obtained from the square antiprism with the extra argon atoms in the middle and above (below) the squares.

The charge transfer found in the SCF calculations of Mg^{2+}-Ar_n, $n = 1−6$, clusters sheds some doubts about the accuracy of the electrostatic expansion for the larger clusters. Therefore, further work is needed, both theoretical and experimental, to elucidate this point.

References and Notes

(1) See articles. In *Physics and Chemistry of Finite Systems: From Clusters to Crystals*; Jena, P., Khanna, S. N., Rao, B. K., Eds.; Kluwer Academic Publishers: Dordrecht, 1992.

(2) Hoare, M. R. *Structure and Dynamics of Simple Microclusters in Advances in Chemical Physics*; Wiley: New York, 1979; Vol. 40.

(3) Vegiri, A.; Farantos, S. C. *J. Chem. Phys.* **1993**, *98*, 4059.

(4) Farantos, S. C.; Kapetanakis, S.; Vegiri, A. *J. Phys. Chem.* **1993**, *97*, 12158.

Potential Functions of Mg^{m+}Ar$_n$ ($m = 1, 2$; $n = 1-18$) Clusters

J. Phys. Chem., Vol. 100, No. 10, 1996 **3909**

(5) Eggen, B. R.; Marks, A. J.; Murrell, J. N.; Farantos, S. C. *Chem. Phys. Lett*. **1994**, *219*, 247.

(6) Farantos, S. C. *Z. Phys. D* **1994**, *31*, 213.

(7) Brechignac, C.; Cahuzac, P.; Carlier, F.; de Frutos, M.; Leygnier, J. *J. Chem. Soc., Faraday Trans*. **1990**, *86*, 2525.

(8) Etters, R. D.; Danilowicz, R.; Dugan, J. *J. Chem. Phys.* **1977**, *67*, 1570.

(9) Pan, R.-P.; Etters, R. D. *J. Chem. Phys*. **1980**, *72*, 1741.

(10) Mistriotis, A. D.; Flytzanis, N.; Farantos, S. C. *Phys. Rev. B* **1989**, *39*, 1212.

(11) Chelikowsky, J. R.; Glassford, K. M.; Phillips, J. C. *Phys. Rev. B* **1991**, *44*, 1538.

(12) Li, S.; Johnston, R. L.; Murrell, J. N. *J. Chem. Soc., Faraday Trans*. **1992**, *88*, 1229.

(13) Velegrakis, M.; Luder, C. *Chem. Phys. Lett*. **1994**, *223*, 139.

(14) Northby, J. A. *J. Chem. Phys*. **1987**, *87*, 6166.

(15) Pilgrim, J. S.; Yeh, C. S.; Berry, K. R.; Duncam, M. A. *J. Chem. Phys.* **1994**, *100*, 7945.

(16) Le Roy, R. J. *J. Chem. Phys*. **1994**, *101*, 10217.

(17) Bauschlicher, C. W., Jr.; Partridge, H.; Langhoff, S. R. *Chem. Phys. Lett*. **1990**, *165*, 272.

(18) Bauschlicher, C. W., Jr.; Partridge, H.; Langhoff, S. R. *J. Chem. Phys.* **1989**, *91*, 4733.

(19) Partridge, H.; Bauschlicher, C. W., Jr.; Langhoff, S. R. *J. Phys. Chem.* **1992**, *96*, 5350.

(20) Bauschlicher, C. W., Jr.; Partridge, H. *Chem. Phys. Lett*. **1995**, *239*, 241.

(21) Eriksson, L. A. *J. Chem. Phys*. **1995**, *103*, 1050.

(22) Patil, S. H. *J. Chem. Phys*. **1991**, *94*, 3586.

(23) MØller, C.; Plesset, M. S. *Phys. Rev.* **1934**, *46*, 618.

(24) Aziz, R. A.; Slaman, M. J. *Mol. Phys.* **1986**, *58*, 679.

(25) GAMESS. *J. Comput. Chem.* **1993**, *14*, 1347.

(26) Farantos, S. C. *Int. Rev. Phys. Chem*., in press.

(27) Shampine, L. F.; Gordon, M. K. *Computer Solutions of Ordinary Differential Equations*; Freeman: San Francisco, 1975.

(28) Papadakis, J.; Fanourgakis, G.; Farantos, S. C. In preparation.

(29) Beguelin, A.; Dongarra, J.; Geist, A.; Jiang, W.; Manchek, R.; Sunderam, V. *PVM 3.0*, Parallel Virtual Machine; ORNL/TM-12187, 1993.

(30) Hinde, R. J.; Berry, R. S.; Wales, D. J. *J. Chem. Phys.* **1992**, *96*, 1376.

(31) Beck, T. L.; Leitner, D. M.; Berry, R. S. *J. Chem. Phys.* **1988**, *89*, 1681.

(32) Gilvarry, J. J. *Phys. Rev.* **1956**, *102*, 308.

(33) Asher, R. L.; Micha, D. A.; Brucat, P. J. *J. Chem. Phys.* **1992**, *96*, 7683.

(34) Chartrand, D. J.; Shelley, J. C.; Le Roy, R. J. *J. Phys. Chem*. **1991**, *95*, 8310.